Interference effect on a heavy Higgs resonance signal in the γγ and ZZ channels

Jeonghyeon Song, Yeo Woong Yoon, and Sunghoon Jung

Interference effect on heavy Higgs resonance signal
in $\gamma\gamma$ and ZZ channels

Jeonghyeon Song,[1,*] Yeo Woong Yoon,[1,2,†] and Sunghoon Jung[2,3,‡]

[1]*School of Physics, KonKuk University, Seoul 143-701, Korea*

[2]*School of Physics, Korea Institute for Advanced Study, Seoul 130-722, Korea*

[3]*SLAC National Accelerator Laboratory, Menlo Park, CA 94025, USA*

Abstract

The resonance-continuum interference is usually neglected when the width of a resonance is small compared to the resonance mass. We re-examine this standard by studying the interference effects in high-resolution decay channels, $\gamma\gamma$ and ZZ, of the heavy Higgs boson H in nearly aligned two-Higgs-doublet models. For the H with a sub-percent width-to-mass ratio, we find that, in the parameter space where the LHC 14 TeV ZZ resonance search can be sensitive, the interference effects can modify the ZZ signal rate by $\mathcal{O}(10)\%$ and the exclusion reach by $\mathcal{O}(10)$ GeV. In other parameter space where the ZZ or $\gamma\gamma$ signal rate is smaller, the LHC 14 TeV reach is absent, but a resonance shape can be much more dramatically changed. In particular, the $\gamma\gamma$ signal rate can change by $\mathcal{O}(100)\%$. Relevant to such parameter space, we suggest variables that can characterize a general resonance shape. We also illustrate the relevance of the width on the interference by adding non-standard decay modes of the heavy Higgs boson.

---

[*] jeonghyeon.song@gmail.com

[†] ywyoon@kias.re.kr

[‡] shjung@slac.stanford.edu

I. INTRODUCTION

Needless to say, the 125 GeV Standard Model (SM) Higgs boson discovery at the LHC Run I [1] is a big step toward the understanding of the electroweak symmetry breaking. But the observed mass of 125 GeV requires a satisfactory explanation for the huge hierarchy between the weak scale and the Planck scale. Most candidate explanations, such as supersymmetry and composite Higgs models, predict a set of new particles at around the electroweak scale. The absence of any such discovery at the LHC Run I motivates us not only to re-ponder naturalness criteria but also to re-visit collider search strategies.

The 13 TeV LHC Run II, which started taking data a few months ago, may indeed need a careful study of resonance searches. Unlike usually assumed, a particle somewhat heavier than the electroweak scale may not show up as a Breit-Wigner (BW) resonance peak at the LHC experiments. The resonance-continuum interference can induce observable impacts on the production rate and the invariant mass distribution (resonance shape). It is generally because (a) a heavier particle can be broader (more decay channels with less phase-space suppression and possible Goldstone enhancements), and (b) the production and decay amplitudes can involve complex phases that arise from SM particles running in loops below the threshold. Various studies have shown that the interference for such cases is not usually negligible [2–25].

Most resonance searches at collider experiments model a resonance as a BW peak and estimate the signal rate by the narrow width approximation (NWA). This is justified if the width-to-mass ratio Γ/M is small enough (see e.g. Ref. [26]) and the resonance width is smaller than the experimental resolution. Thus, LHC searches assume 1% Γ/M in the $\gamma\gamma$ channel [27, 28] and 0.5% in the ZZ channel [29, 30], which imply that the width of a few hundred GeV resonance is similar or smaller than the experimental bin size. But for even a slightly broader resonance, perhaps with some complex phases in its production and decay amplitudes, such approximation may not be guaranteed. In this paper, we re-examine such approximation using the two-Higgs-doublet models (2HDM).

A notable example that reveals the dramatic interference effect is the decay of heavy Higgs bosons H and A into the $t\bar{t}$ at hadron colliders [3]. Most strikingly, it was shown that a pure resonance dip is produced in a large part of parameter space [4]. In other parameter space, a general mixture of the real- and the imaginary-part interferences produces a mixture

of a peak and a dip in the $m_{t\bar{t}}$ distribution [4, 31, 32]. Unfortunately, it is difficult to resolve such rich structure of the $t\bar{t}$ resonance shape [31] because the experimental $m_{t\bar{t}}$ resolution ~ 100 GeV [33, 34] is bigger than the typical width of the heavy Higgs bosons in the aligned 2HDM. Although a pure dip can perhaps be well searched using the available techniques optimized for a BW peak [4], it is produced only in some part of the parameter space.

The interference also exists in the high-resolution decay channels, $\gamma\gamma$ and ZZ. The interferences of the SM-like heavy Higgs boson at hadron colliders, $gg \to H \to ZZ, \gamma\gamma$, have been calculated in last decades [5, 6, 10, 12–16, 21]; but they are found to be insignificant producing mostly a BW peak. The main difference between the $t\bar{t}$ and $ZZ, \gamma\gamma$ channels is the relative size of the continuum and the resonance processes [4]. The $t\bar{t}$ experiences a significant interference because the tree-level continuum, B, and the one-loop resonance, S, can produce a loop-factor enhanced interference $\sqrt{SB}/S \sim \sqrt{B/S}$ relative to the resonance-squared. While large interference effects might be expected in $gg \to \gamma\gamma$ since the continuum produced by a one-loop process whereas the resonance process occurs via two-loops, small interference effects are expected in $gg \to ZZ$ since both continuum and resonance processes are one-loop order. Meanwhile, the off-shell interference of the SM Higgs, which is beyond the scope of this paper, with the continuum ZZ at an invariant mass much bigger than 125 GeV was found to be sensitive to the Higgs width [12, 35, 36].

Nonetheless, the interference in the ZZ and $\gamma\gamma$ can be more exciting for the 2HDM heavy Higgs bosons. The expectation is again based on a general estimation of the relative interference [4]. In the nearly-aligned 2HDM, as is preferred by SM Higgs precision measurements ($|c_{\beta-\alpha}| \lesssim 0.1 - 0.4$ depending on models), the resonance process is suppressed by the small $c_{\beta-\alpha}$ and complex phases can be different in the $\gamma\gamma$ channel as the W boson loop is suppressed. As a result, the interference can be relatively enhanced and the resonance shape can be non-trivially modified. Thus, we study the interference in the ZZ and $\gamma\gamma$ channels in this nearly-aligned 2HDM. This setup is not only motivated by Higgs precision measurements, but can illustrate the resonance-continuum interference of a relatively narrow resonance.

The paper is organized as follows. In Sec. II, we review the 2HDM and our formalism of the interference effect on the invariant mass distribution. In addition, we suggest a few variables that can characterize a resonance shape containing a peak and a dip. We then present the results for the $\gamma\gamma$ channel in Sec. III and the ZZ channel in Sec. IV. We also consider the case of a somewhat broader heavy Higgs boson in Sec. V, in which we add

non-standard decay modes. Section VI contains our conclusions.

II. BRIEF REVIEW OF THE 2HDM AND THE INTERFERENCE EFFECTS

A. H in the 2HDM

We consider a 2HDM [37] with CP invariance and softly broken Z_2 symmetry, which introduces two complex Higgs doublet scalar fields, Φ_1 and Φ_2, where

$$\Phi_j \equiv \begin{pmatrix} \phi_j^+ \\ \frac{1}{\sqrt{2}}\left(v_j + \rho_j^0 + i\eta_j^0\right) \end{pmatrix}, \tag{1}$$

with $v_1 = v\cos\beta, v_2 = v\sin\beta$, and $v = 246\,\text{GeV}$. The electroweak symmetry breaking is generated by non-zero vacuum expectation value v of a linear combination $H_1 = \cos\beta\Phi_1 + \sin\beta\Phi_2$. Its orthogonal combination $H_2 = -\sin\beta\Phi_1 + \cos\beta\Phi_2$ acquires zero vacuum expectation value. In what follows, we take $s_x = \sin x$, $c_x = \cos x$, and $t_x = \tan x$ for notational simplicity. There are five physical Higgs boson degrees of freedom, the light CP-even scalar h $(= -s_\alpha\rho_1^0 + c_\alpha\rho_2^0)$, the heavy CP-even scalar H $(= c_\alpha\rho_1^0 + s_\alpha\rho_2^0)$, the CP-odd pseudoscalar A $(= -s_\beta\eta_1^0 + c_\beta\eta_2^0)$, and two charged Higgs bosons $H^\pm$ $(= -s_\beta\phi_1^\pm + c_\beta\phi_2^\pm)$, where α is the mixing angle between CP-even Higgses. The SM Higgs field is the CP-even neutral state of H_1:

$$H^{\text{SM}} = s_{\beta-\alpha}h + c_{\beta-\alpha}H. \tag{2}$$

Note that if $s_{\beta-\alpha} = 1$, h has the same couplings as the SM Higgs boson, which is preferred by the SM Higgs precision measurement with LHC8 data [38]. This is called the alignment limit [39].

We consider the case where the observed 125 GeV state H^{SM} is the lighter CP-even state h although another interesting possibility of $H^{\text{SM}} = H$ is still compatible with the current LHC Higgs data [40–46]. In addition, we assume $s_{\beta-\alpha} > 0$[1]. Focused on $\gamma\gamma$ and ZZ decay modes, we study the gluon fusion production of H in the two-dimensional parameter space of M_H and t_β with the given $c_{\beta-\alpha}$. Another model parameter, the soft Z_2 symmetry breaking term m_{12}^2, is tuned to suppress H-h-h triple coupling λ_{Hhh}, where

$$\lambda_{Hhh} = \frac{c_{\beta-\alpha}}{vs_{2\beta}}\left\{\left(\frac{6s_{2\alpha}}{s_{2\beta}} - 2\right)m_{12}^2 - s_{2\alpha}\left(M_H^2 + 2m_h^2\right)\right\}. \tag{3}$$

---

[1] Note that the wrong sign case in the 2HDM is shown to be still allowed by the current LHC Higgs signal strength measurements, though less probable [46].
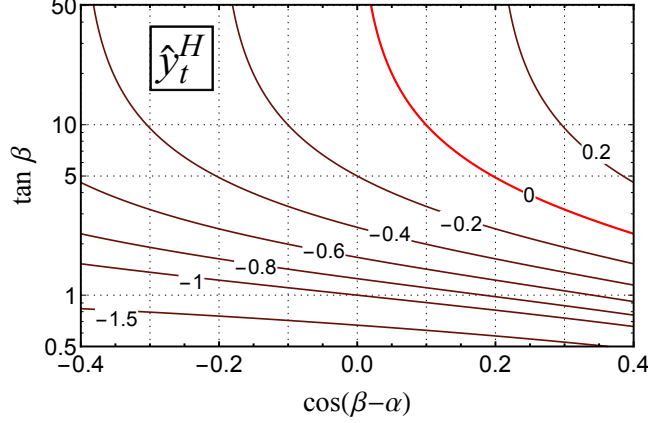
4

FIG. 1. The top quark Yukawa coupling $\hat{y}_t^H$ normalized by the SM one is shown in the $(c_{\beta-\alpha}, t_\beta)$ plane for $s_{\beta-\alpha} > 0$. We mark the top-phobic $\hat{y}_t^H = 0$ contour with brighter red.

The H-V-V ($V = W^\pm, Z$) coupling normalized by the SM value is $c_{\beta-\alpha}$. In order to have $H \to ZZ$, therefore, we need some deviation from the alignment limit. We will therefore consider 'nearly aligned' 2HDM in the remainder of this work.

Yukawa couplings, which play an important role in Higgs phenomenology, are different among the types of 2HDM. In this study, we consider Type I and Type II where the normalized Yukawa couplings by the SM values, $\hat{y}_{t,b,\tau}^H$, in terms of $c_{\beta-\alpha}$ and $s_{\beta-\alpha}$ are

$$
\begin{array}{c|cc}
 & c_{\beta-\alpha} - \dfrac{s_{\beta-\alpha}}{t_\beta} & c_{\beta-\alpha} + t_\beta s_{\beta-\alpha} \\
\hline
\text{Type I} & \hat{y}_t^H, \hat{y}_b^H, \hat{y}_\tau^H & \\
\text{Type II} & \hat{y}_t^H & \hat{y}_b^H, \hat{y}_\tau^H
\end{array}
\tag{4}
$$

Note that both Type I and Type II have the same top quark Yukawa coupling.

We find that there exist a special parameter choice for $\hat{y}_t^H = 0$, called the top-phobic H. To be more specific, we present the value of $\hat{y}_t^H$ in the parameter space of $(c_{\beta-\alpha}, t_\beta)$ in Fig. 1. As the red line indicates, a specific *nonzero positive* $c_{\beta-\alpha}$ for a given t_β leads to vanishing $\hat{y}_t^H$, which happens, for example, when $t_\beta = 10$ for $c_{\beta-\alpha} = 0.1$ or $t_\beta = 2.3$ for $c_{\beta-\alpha} = 0.4$. Near the top-phobic line the signal rate is severely suppressed especially for Type I.

B. General formalism for interference

We consider the interference between the continuum background and the resonance process of a particle with mass M and total decay width Γ in a $2 \to 2$ scattering process. When

we write the helicity amplitudes for the continuum background ($\mathcal{M}_{\rm cont}$) and the resonance ($\mathcal{M}_{\rm res}$) as

$$\mathcal{M}_{\rm cont} = \mathcal{A}_{\rm cont} e^{i\phi_{\rm cont}}, \tag{5}$$
$$\mathcal{M}_{\rm res} = \frac{M^2}{\hat{s} - M^2 + iM\Gamma}\, \mathcal{A}_{\rm res} e^{i\phi_{\rm res}},$$

the total partonic cross-section becomes

$$\hat{\sigma}_{\rm cont} + \hat{\sigma}_{\rm sig} = \hat{\sigma}_{\rm cont} + \hat{\sigma}_{\rm res}\frac{M^4}{(\hat{s} - M^2)^2 + M^4 w^2}\left[1 + \frac{2w}{R}\sin\phi + \frac{2(\hat{s} - M^2)}{M^2}\frac{\cos\phi}{R}\right] \tag{6}$$
$$\equiv \hat{\sigma}_{\rm cont} + \hat{\sigma}_{\rm res}\Big[f_{\rm BW}(m_{\rm inv}) + f_{\rm Im}(m_{\rm inv}) + f_{\rm Re}(m_{\rm inv})\Big],$$

where $m_{\rm inv} = \sqrt{\hat{s}}$. Note that $f_{\rm BW}, f_{\rm Im}, f_{\rm Re}$ take the terms in square bracket one by one. $\hat{\sigma}_{\rm cont}$, $\hat{\sigma}_{\rm res}$, R, and the interference phase ϕ are

$$\hat{\sigma}_{\rm cont,res} = \frac{1}{32\pi\hat{s}}\int dz \sum \mathcal{A}^2_{\rm cont,res}, \tag{7}$$
$$\hat{\sigma}_{\rm int} e^{i\phi} = \frac{1}{32\pi\hat{s}}\int dz \sum \mathcal{A}_{\rm cont}\mathcal{A}_{\rm res} e^{i(\phi_{\rm res} - \phi_{\rm cont})},$$
$$R = \frac{\hat{\sigma}_{\rm res}}{\hat{\sigma}_{\rm int}}, \quad w \equiv \frac{\Gamma}{M},$$

where $z = \cos\theta^*$ while θ^* is the scattering angle in the c.m. frame. The summation is over helicity and color indices. R, w, and ϕ are the key parameters which determine the pattern of interference effect. More intuitive form for R and ϕ can be obtained if assuming that one helicity amplitude is dominant:

$$R \simeq \frac{\mathcal{A}_{\rm res}}{\mathcal{A}_{\rm cont}}, \quad \phi \simeq \phi_{\rm res} - \phi_{\rm cont}. \tag{8}$$

As can be understood from Eq. (6) and will be discussed more, w/R indicates the strength of interference effect and ϕ determines whether it is imaginary-part interference ($c_\phi = 0$) or real-part interference ($s_\phi = 0$), or between the two.

Most of new particles of our interest have narrow width ($w \ll 1$), which confines the signal events in the resonance region of the invariant mass distribution. It is a good approximation to ignore the $m_{\rm inv}$ dependence of R and ϕ. Then $m_{\rm inv}$ dependence of $\hat{\sigma}_{\rm sig}$ is explicitly shown in Eq. (6) as a simple function of $\hat{s}\ (= m_{\rm inv}^2)$. Apparently, $f_{\rm Re}(m_{\rm inv})$ is an odd function at $m_{\rm inv} = M$, which yields a dip-peak or peak-dip structure. On the contrary $f_{\rm BW}(m_{\rm inv})$ and $f_{\rm Im}(m_{\rm inv})$ are even functions. The sensitivity to $f_{\rm Re}(m_{\rm inv})$ and $f_{\rm Im}(m_{\rm inv})$ crucially depends on the bin size of the invariant mass distribution. If the bin is large such that a dip-peak
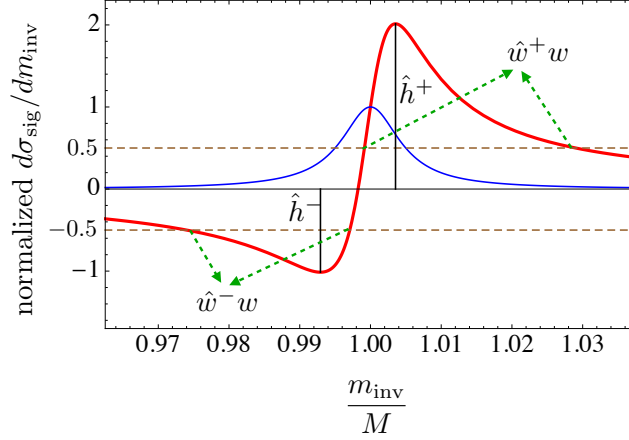
FIG. 2. The definitions of variables characterizing a resonance shape in Eq. (10): the relative height $\hat{h}^+$ and depth $\hat{h}^-$, the relative peak width $\hat{w}^+$, and the relative dip width $\hat{w}^-$ for $w = 0.01$, $R = 0.007$, and $\phi = 0$. We normalized the differential cross section about the invariant mass such that the peak height of the BW resonance without any interference (blue) is a unity.

structure is included in one bin, we should integrate over m_{inv}, which eliminates the real-part interference. If the bin is narrow enough, more dynamic structure of f_{Re} can be probed. We consider these two cases and suggest new observation factors for each case.

(i) Large bin: In this case, we integrate $\hat{\sigma}_{\text{sig}}$ over m_{inv}, under which the even functions survive but the odd function $f_{\text{Re}}(m_{\text{inv}})$ is washed out at leading order[2]. The survived imaginary part interference results in a multiplicative factor, $(1 + 2w \sin\phi/R)$, to the NWA rate $\sigma \cdot \text{Br}$. Therefore, the total signal rate can significantly differ from what obtained from the NWA due to the imaginary part interference. In Ref. [4], we called this as the correction factor $C (\equiv 1 + \Delta C)$:

$$C \equiv \frac{\sigma_{\text{mNWA}}}{\sigma_{\text{prod}} \cdot \text{Br}} = 1 + \frac{2w}{R} \sin\phi \,, \tag{9}$$

where σ_{mNWA}, whose subscript denotes *modified* NWA, is the total signal rate by including imaginary-part interference effect. In the pure imaginary case ($\cos\phi = 0$) there are three unique shapes of a resonance: a pure dip ($C < 0$), a pure peak ($C > 0$), or a nothingness ($C = 0$). Note that the C factor is measurable by comparing the observed event rate with the simulation result of $\sigma_{\text{prod}} \cdot \text{Br}$.

(ii) Fine bin: In an ideal situation with very small bin size, the m_{inv} dependence of σ_{sig} can be measured, which is more crucial in observing the dip-peak structure with nonzero

---

[2] Of course, the cancelation is not perfect because of the strong $\hat{s}$ dependence of the gluon luminosity.

7

real-part interference. When $\cos\phi \neq 0$, the full resonance shape of $\hat\sigma_{\mathrm{sig}}(m_{\mathrm{inv}})$ is a dip-peak (peak-dip) structure if $\mathrm{sign}(\cos\phi) = +1(-1)$. In order to quantify the signal rates of the dip and peak, we define the relative height $\hat{h}^+$ and depth $\hat{h}^-$, compared with the height of the BW peak. In addition, the relative widths of the peak and dip are defined as $\hat{w}^\pm$, as illustrated in Fig. 2. For the general case with both real- and imaginary-part interference, we obtain $\hat{h}^\pm$ and $\hat{w}^\pm$ in terms of our key parameters as

$$\hat{h}^\pm = \frac{1}{2}\left[\sqrt{C^2 + \left(\frac{2w\cos\phi}{R}\right)^2} \pm C\right],$$ (10)

$$\hat{w}^\pm = \sqrt{\left(\frac{2w\cos\phi}{R}\right)^2 - 1 \pm 2C}.$$

Note that $\hat{w}^-$ is not defined if $(2w\cos\phi/R)^2 < 1+2C$ when $C > 0$: this is because we defined $\hat{w}^-$ as the width at the negative half-maximum of the BW one. If the dip is shallow such that its depth is smaller than the BW half-maximum, we do not calculate $\hat{w}^-$ as considering it as a shallow dip.

Two limiting cases ($2w/R \ll 1$ and $2w/R \gg 1$) present a clear understanding of the real part interference effect. When $\sin\phi = 0$, Eq. (10) to leading order becomes

$$\hat{h}^+ \simeq \hat{h}^- \simeq \frac{w}{R}, \qquad \hat{w}^+ \simeq \hat{w}^+ \simeq \frac{2w}{R}, \qquad \text{if } \frac{2w}{R} \gg 1;$$ (11)

$$\hat{h}^+ \simeq 1, \quad \hat{h}^- \simeq 0, \quad \hat{w}^+ \simeq 1, \qquad \text{if } \frac{2w}{R} \ll 1.$$ (12)

It is clear that the total width is not the key parameter which determines the real part interference, but the ratio w/R is. Even though Γ is very small compared to its mass M, smaller R can make the ratio w/R large: we have a profound dip-peak structure with enhanced height and enhanced width: see Eq. (11). If $w/R \ll 1$, we have a very shallow dip and a BW-like peak as shown in Eq. (12).

On the analogy of the correction factor C, which quantifies the integrated NP signal rate with the interference, we suggest two new factors, the distribution factors D^+ and D^-, defined by

$$D^\pm = \hat{h}^\pm \hat{w}^\pm.$$ (13)

Note that $D^\pm$ is not exactly proportional to the new physics signal rate, since the resonance shape with interference is different from the ordinary BW form. However these simple factors

provide a powerful estimate for the dip-peak structure, especially useful when scanning a theoretical parameter space in order to look for large real-part interference effect. If $D^- = 1$ for example, we can expect that a dip shall appear with almost the same rate with the BW resonance.

III. $\gamma\gamma$ CHANNEL

The diphoton decay channel of a heavy neutral Higgs boson H produced by the gluon-gluon fusion is a two loop process while the SM continuum background $gg \to \gamma\gamma$ is a one loop process[3]. The parton level differential cross section of $gg \to \gamma\gamma$ is

$$\frac{d\hat{\sigma}(gg \to \gamma\gamma)}{dz} = \frac{1}{32\pi\hat{s}} \frac{\alpha_s^2 \alpha_e^2}{2} \sum_{\lambda_1\lambda_2\lambda_3\lambda_4} \left| \mathcal{M}^{\text{cont}}_{\lambda_1\lambda_2\lambda_3\lambda_4} + \mathcal{M}^{H}_{\lambda_1\lambda_2\lambda_3\lambda_4} \right|^2 , \tag{14}$$

where $\mathcal{M}^{\text{cont},H}_{\lambda_1\lambda_2\lambda_3\lambda_4}$ are the normalized helicity amplitudes from the continuum background and H resonance with the helicity of incoming gluons (λ_1, λ_2) and outgoing photons (λ_3, λ_4). The overall factor is due to the loop correction. We refer the explicit expressions of $\mathcal{M}^{\text{cont}}$'s to Refs. [21, 47]. For the Higgs resonance signal $gg \to H \to \gamma\gamma$, only four helicity amplitudes are nonzero:

$$\mathcal{M}^{H}_{++++} = \mathcal{M}^{H}_{----} = \mathcal{M}^{H}_{++--} = \mathcal{M}^{H}_{--++}$$
$$= \frac{G_F}{128\pi^2} \frac{\hat{s}^2}{\hat{s} - M_H^2 + iM_H\Gamma_H} \sum_q \hat{y}_q^H A_{1/2}^H (\tau_q)$$
$$\times \left(\sum_q \hat{y}_q^H N_c Q_q^2 A_{1/2}^H (\tau_q) + \sum_\ell \hat{y}_\ell^H Q_\ell^2 A_{1/2}^H (\tau_\ell) + c_{\beta-\alpha} A_1^H(\tau_W) \right), \tag{15}$$

where $\tau_p = \hat{s}/(4m_p^2)$, and $\hat{y}_{q,\ell}^H$'s are shown in Eq. (4), and the expressions of $A_{1/2,1}^H(\tau)$ are in Ref. [48].

We first study the relative complex phase ϕ. The complex phase arises through the loop diagrams when the squared of the momentum that passes through an internal cut line is greater than the threshold mass square in the loop. The continuum background $gg \to \gamma\gamma$ is dominated by light quark (u, d, s, c, b) loops whose complex phase arises in $(+-+-), (-+-+), (+--+), (-++-)$ helicity amplitudes. But, those helicity amplitudes do not inference with the Higgs resonance amplitudes as can be clearly seen in Eq. (15).

---

[3] We do not consider subdominant two-loop contribution in continuum background. Its effect on the resonance-continuum interference was shown to be 5% when $M_H < 160\,\text{GeV}$ [5, 49].
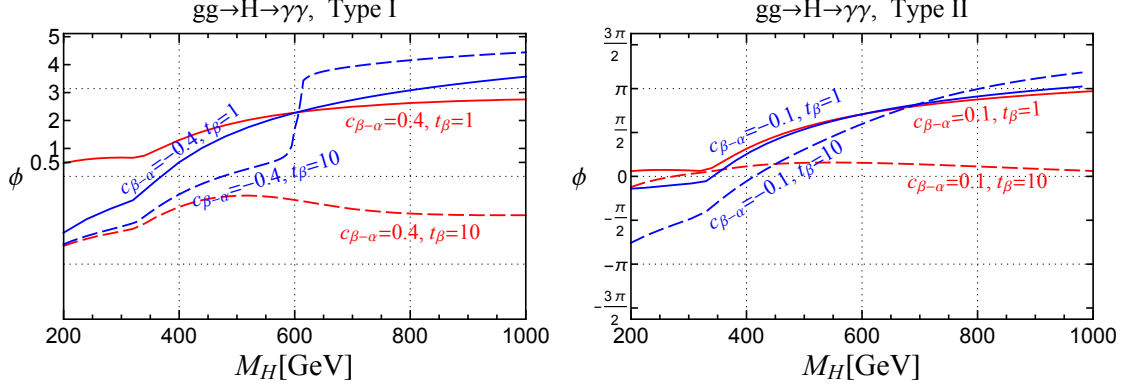
FIG. 3. The resonance-continuum interference phase ϕ of the $gg \to (H \to)\gamma\gamma$ process for various benchmark parameter values of $c_{\beta-\alpha}$ and t_β in the Type I (left panel) and Type II (right panel) models. The abrupt change at around $M_H \simeq 2m_t$ is due to the onset of top-pair threshold.

Then, only the top quark loop can give small contribution to the complex phase. The relative phase ϕ is mainly from the Higgs resonance. $gg \to H \to \gamma\gamma$ is dominated by top quark loop and W boson loop where the latter is suppressed for small $c_{\beta-\alpha}$. When $M_H < 2m_t$ the imaginary part of amplitude arises mostly from the W loop while after $M_H > 2m_t$ from the top quark loop. If both $c_{\beta-\alpha}$ and $\hat{y}_t^H$ are positive like the SM Higgs boson, two contributions are destructive.

In Fig. 3, we show ϕ with respect to M_H for several benchmark parameter points of $c_{\beta-\alpha}$ and t_β. We set $c_{\beta-\alpha} = \pm 0.4$ for Type I and $c_{\beta-\alpha} = \pm 0.1$ for Type II, which are marginally allowed by the current Higgs precision measurement. In both Types, there is a considerable portion of parameter space where the imaginary-part interference is large, i.e., sizable $\sin\phi$.

For Type I, we consider four cases of $c_{\beta-\alpha} = \pm 0.4$ and $t_\beta = 1, 10$. The value of ϕ is determined by the behaviors of the real and imaginary parts of the loop functions at the given mass M_H. For example, let us focus on $M_H = 200$ GeV where W loop mainly generates a phase. The case $(c_{\beta-\alpha} = 0.4, t_\beta = 1)$ has ϕ near zero while the other three cases have large negative values near $-\pi/2$. As shown in Fig. 1, $(c_{\beta-\alpha} = 0.4, t_\beta = 1)$ leads to negative $\hat{y}_t$ so that the top quark loop and the W loop become constructive: the real part of the total loop function become larger; the phase ϕ is small. For the other three cases, the destructive interference reduces the real parts of the loop function significantly. The untouched imaginary loop function part, which is negative in these cases, yields $\phi \sim -\pi/2$. For other M_H, similar understanding is possible through the relative strengths and signs of $\hat{y}_{t,b}$ and $c_{\beta-\alpha}$. The abrupt change of amount π in ϕ at $M_H = 600$ GeV for $c_{\beta-\alpha} = -0.4$

10

and $t_\beta = 10$ is attributed to the cancelation of two real-parts between W and top loops and consequent sign flip.

For Type II, the four cases of $c_{\beta-\alpha} = \pm 0.1$ and $t_\beta = 1, 10$ are considered. The small values of $c_{\beta-\alpha} = \pm 0.1$ suppress the W loop contribution. The imaginary phase occurs in the loop function $A_{1/2}^H(\tau_t)$ when $M_H > 2m_t$. For $M_H < 2m_t$, ϕ is close to zero except for the case $(c_{\beta-\alpha} = -0.1, t_\beta = 10)$ where the sizable b quark contribution with large t_β considerably cancels the whole real part and ϕ has large negative value. As M_H crosses the $2m_t$ threshold, ϕ continually increases up to π except for $(c_{\beta-\alpha} = 0.1, t_\beta = 10)$ case. Here the real part of $A_{1/2}^H(\tau_t)$ vanishes when $M_H = 1.1$ TeV so that one loop function generates the phase of $\pi/2$. Two factors of $A_{1/2}^H(\tau_t)$ from production and decay processes yields $\phi = \pi$. The exceptional $(c_{\beta-\alpha} = 0.1, t_\beta = 10)$ case is near the top-phobic line. In this case, real parts of W loop and bottom quark loop are added up while some cancelation arise for imaginary part. Therefore, ϕ is very small along the whole M_H region.

Secondly we examine w and R in $gg \to \gamma\gamma$, of which the ratio w/R is the crucial factor to determine the interference effects. For simplicity, we assume that H decays into $WW, ZZ, q\bar{q}, \tau\tau, \gamma\gamma$. The possibly important decay channel $H \to hh$ is neglected, which can be achieved by tuning the soft Z_2 symmetry breaking term m_{12}^2. Since this assumption minimizes the total width and thus the interference effects, it shows a good limiting feature of the interference effects in $gg \to \gamma\gamma$. The effect of additional decay channels shall be discussed in Sec. V. Under this assumption, the Γ_H, which generally increases with M_H, depends on $c_{\beta-\alpha}$ and t_β. If $c_{\beta-\alpha} = \pm 0.1$, the parameter w for $M_H \lesssim 1$ TeV is very small to be $\mathcal{O}(10^{-3}) - \mathcal{O}(10^{-2})$ depending on the t_β value since $H \to WW, ZZ$ is very suppressed. If $c_{\beta-\alpha} = \pm 0.4$ the WW, ZZ decay channels becomes quite significant so that Γ_H can be $100\,\text{GeV}$ until $M_H < 1\,\text{TeV}$.

The R value, proportional to the ratio of the magnitude of the signal amplitude to that of the background amplitude, is generically small in $gg \to \gamma\gamma$. The background process is at one loop and the H signal is at two loop. The ratio R is roughly one-loop suppressed. In most of the parameter space R is less than 10^{-3}. We have very large interference effects.

Now we quantitatively discuss the interference effects. In Fig. 4, we show the contour plots for C factor as well as the modified total signal rate $\sigma_{\text{mNWA}} = C \times (\sigma \cdot \text{Br})$ at $14\,\text{TeV}$ in (M_H, t_β) plane for $c_{\beta-\alpha} = \pm 0.4$ in Type I and $c_{\beta-\alpha} = \pm 0.1$ in Type II. For the initial gluon luminosity, we used CT10NLO PDF set [50]. We also applied NNLO k-factor to the
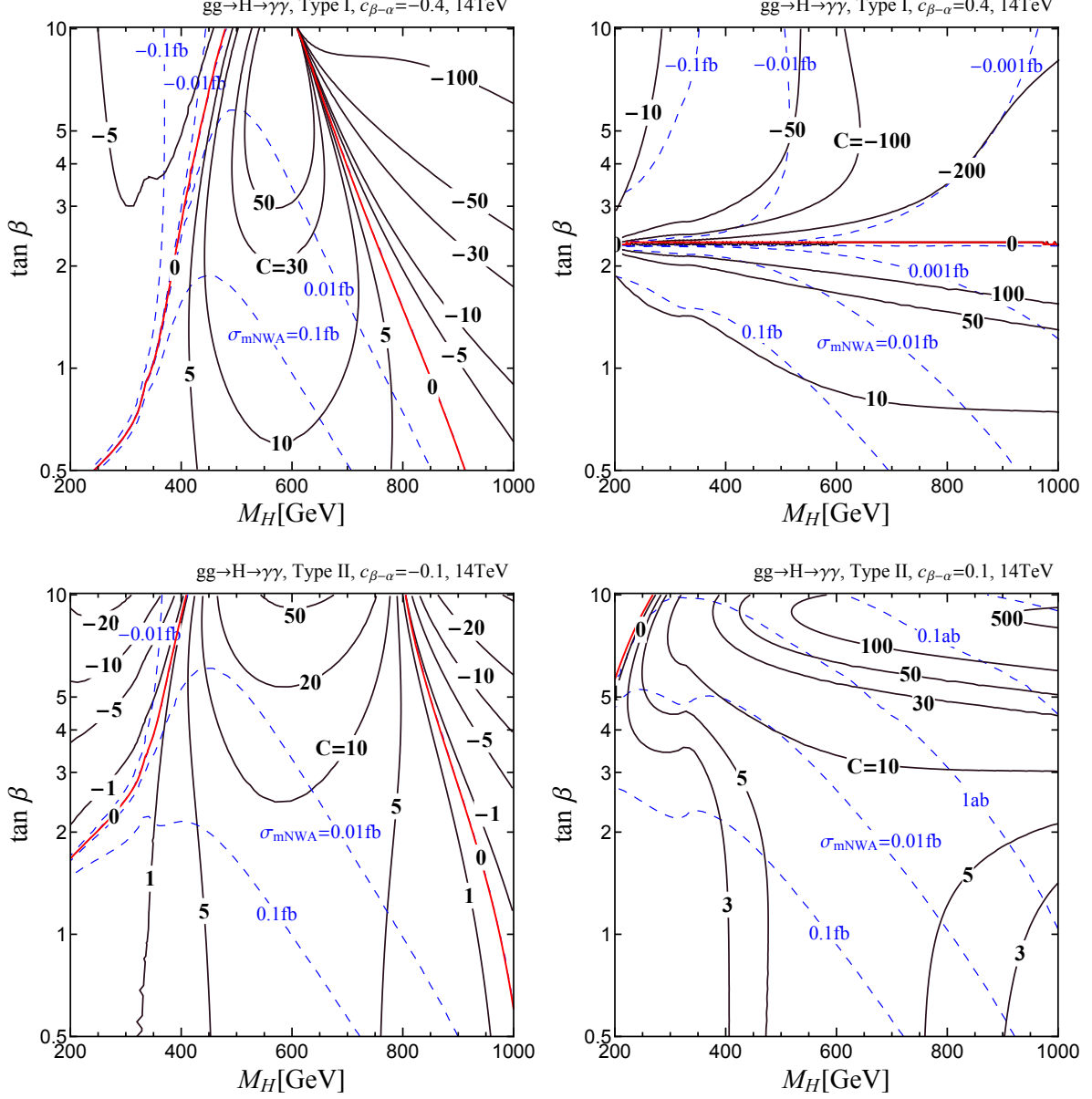
FIG. 4. Contours of the C factor (solid black) and the σ_{mNWA} (dashed blue) of the $gg \to H \to \gamma\gamma$ process at the LHC 14 TeV in the (M_H, t_β) plane. The contour of $C = 0$ is marked with red-solid.

heavy Higgs resonance production part using `HIGLU` fortran package [51] and use the LO decay rate of heavy Higgs in Ref. [52].

The most unexpected result is that the interference effect $|\Delta C|$ can be $\mathcal{O}(100)\%$ even when w is sub-percent level ($c_{\beta-\alpha} = \pm 0.1$ and large t_β). The usually adopted criteria to ignore the interference effect, $w \ll 1$, is not good enough. The characteristics of C values for different type and parameters are as follows. The C contours for $c_{\beta-\alpha} < 0$ show some common features in both Type I and Type II. They have three sectors divided by two

$C = 0$ lines. The left and right parts of these lines have large negative C factors (dip-like resonance shapes), while the middle region has positive C factors (peak-like resonance shapes). The two $C = 0$ lines appear near two points $\phi \simeq 0$ and $\phi \simeq \pi$, where ΔC flips its sign (here $2w/R$ is very large). As shown in Fig. 3(b), crossing $\phi = 0, \pi$ happens two times for $200\,\mathrm{GeV} < M_H < 1\,\mathrm{TeV}$, which passes near two $C = 0$ lines. In addition, the magnitude of C increases with increasing t_β. This is because the signal amplitude (or R) is reduced by increasing t_β. On the contrary σ_{mNWA} decreases with increasing t_β. In the Type II $c_{\beta-\alpha} = 0.1$ case, there is only one $C = 0$ line since ϕ crosses $\phi = 0$ point once when $t_\beta = 10$: see Fig. 3(b).

For the $c_{\beta-\alpha} > 0$ case of Type I, there is one horizontal $C = 0$ line. However the origin of $C = 0$ here is different from the other three cases. It is very close to the top-phobic (actually fermion-phobic due to the common $\hat{y}^H$'s for all fermions) line as in Fig. 1. This fermion-phobic nature prohibits the gluon fusion production itself. In the vicinity of the $C = 0$ line, very small R is generated, enhancing C extremely. Since the sign of top Yukawa coupling is flipped at this line, so does the sign of C. Another unexpected result is that the large t_β region in Type I has compatible signal rate with the small t_β region since $\hat{y}_t^H$ increases again with t_β after crossing the top-phobic line. Our final observation is that $|\Delta C|$ and σ_{mNWA} are anti-correlated in general: the region for large $|\Delta C|$ usually has very suppressed signal rate.

IV. ZZ CHANNEL

For the ZZ channel, both the SM background process $gg \to ZZ$ and the Higgs resonance signal $gg \to H \to ZZ$ are one-loop processes. The partonic differential cross section is

$$\frac{d\hat{\sigma}(gg \to ZZ)}{dz} = \frac{1}{32\pi\hat{s}} \frac{\alpha_s^2 \alpha_Z^2 \beta_Z}{256} \sum_{\lambda_1 \lambda_2 \lambda_3 \lambda_4} |\mathcal{T}_{\lambda_1 \lambda_2 \lambda_3 \lambda_4}^{\mathrm{cont}} + \mathcal{T}_{\lambda_1 \lambda_2 \lambda_3 \lambda_4}^{H}|^2, \tag{16}$$

where $\alpha_Z = \alpha_e/(\sin^2\theta_W \cos^2\theta_W)$ with weak mixing angle θ_W and $\beta_Z = \sqrt{1 - 4m_Z^2/\hat{s}}$. $\mathcal{T}^{\mathrm{cont}}$ and $\mathcal{T}^H$ are the normalized helicity amplitude for the background and H signal, respectively, of which the expressions are referred to Ref. [8][4]. A big difference between $\mathcal{T}^{\mathrm{cont}}(gg \to ZZ)$ and $\mathcal{M}^{\mathrm{cont}}(gg \to \gamma\gamma)$ is the presence of the longitudinal mode in the ZZ channel.

---

[4] $\mathcal{T}_{\lambda_1 \lambda_2 \lambda_3 \lambda_4}$ are corresponding to $\mathcal{M}_{\lambda_1 \lambda_2 \lambda_3 \lambda_4}$ in Ref. [8]. There is an obvious typo in Eq. (3.14) of Ref. [8] since the mass dimensions of the first two terms in curly brackets of right hand side are incorrect. From the independent calculation, we find that it should be $(1+\beta)\{4s(t-u)Y/(s_4 u_1 t_1) + 4Y/s_4 (...) + ...\}$ where the ellipsis represent the same form of the equation.

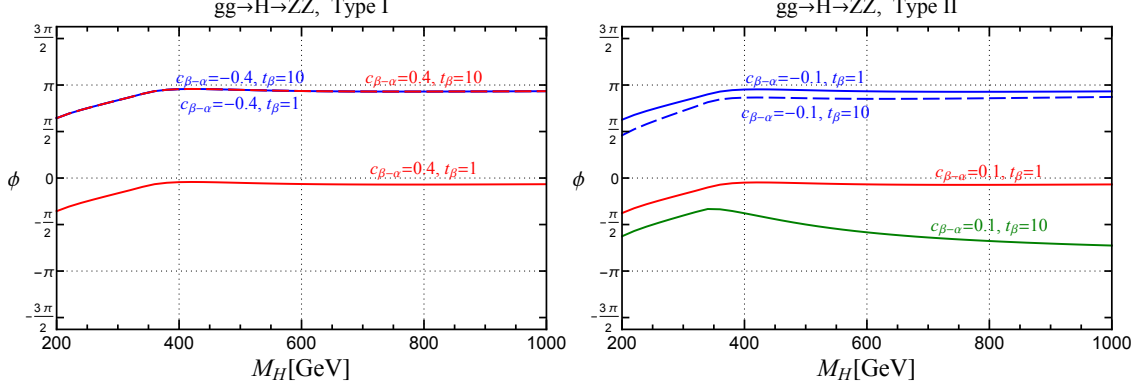FIG. 5. The resonance-continuum interference phase ϕ of the $gg \to (H \to)ZZ$ process for various benchmark parameter values of $c_{\beta-\alpha}$ and t_β in the Type I (left panel) and Type II (right panel) models. The abrupt change at around $M_H \simeq 2m_t$ is due to the onset of top-pair threshold. The top-phobic case is shown as the green-solid.

In particular when both outgoing Z bosons are longitudinal (called the LL mode), the amplitude is proportional to m_q^2. In the ZZ mode, therefore, the top quark contribution becomes important after the $t\bar{t}$ threshold. We found that the LL contribution increases linearly with m_{ZZ}, reaching about 50% at $m_{ZZ} = 700\,\text{GeV}$.

We first study the complex phase ϕ in ZZ channel. For the background process, the complex phase from the top quark loop significantly increases with invariant mass m_{ZZ} after the $t\bar{t}$ threshold while the light quark contribution to ϕ_{cont} decreases quickly. For $gg \to H \to ZZ$, the top quark loop contribution to $gg \to H$ provides dominant complex phase unless b contribution becomes dominant for large t_β in Type II. It appears that the behaviors of complex phases of the top loop contributions from $gg \to ZZ$ and $gg \to H \to ZZ$ are quite similar after $M_H > 2m_t$. As a result, the phase $\phi \sim (\phi_{\text{res}} - \phi_{\text{cont}})$ is close to 0 or π depending on overall sign. This is clearly shown in Fig. 5. One exception is the case $(c_{\beta-\alpha} = 0.1, t_\beta = 10)$ in Type II (green-colored line), which corresponds to top-phobic H: ϕ is quite different from 0 or π. Here the bottom quark loop is dominant. We also found that Type I shows special behavior: only two curves appear regardless of $c_{\beta-\alpha}$ and t_β. It is because all $\hat{y}^H$'s are the same and thus ϕ_{res} is also the same except the overall sign. For example, $c_{\beta-\alpha}\hat{y}^H$ in the case $(c_{\beta-\alpha} = 0.4, t_\beta = 1)$ has opposite sign of that in the other three cases: see Fig. 1.

Now, we investigate C factor and σ_{mNWA}. Basic setup is similar to $\gamma\gamma$ channel. The w parameter is small in general. The R is roughly $\mathcal{O}(0.01)$, mostly larger than w, since both
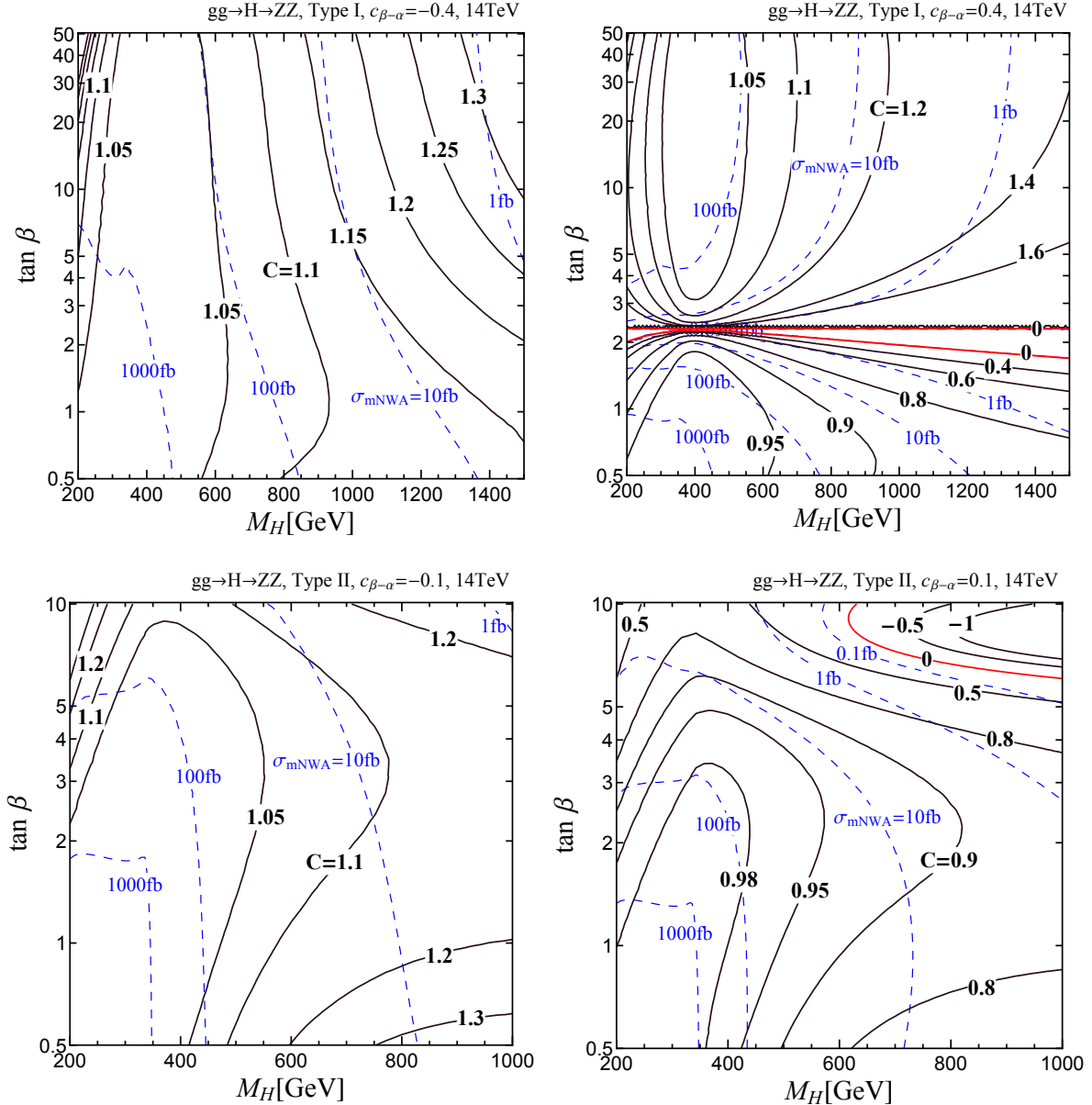
FIG. 6. Contours of the C factor (solid black) and the σ_{mNWA} (dashed blue) of the $gg \to H \to ZZ$ process at the LHC 14 TeV in the (M_H, t_β) plane. The contour of $C = 0$ is marked with red-solid.

the SM background process and the Higgs resonance signal are one-loop processes. The interference effect would be generically small in ZZ channel for small w. Moreover the $c_{\beta-\alpha}$ value does not affect the ratio w/R much since larger $c_{\beta-\alpha}$ increases both R and w.

In Fig. 6, we show the contours of the C factor and σ_{mNWA} in (M_H, t_β) plane for $c_{\beta-\alpha} = \pm 0.4$ for Type I and $c_{\beta-\alpha} = \pm 0.1$ for Type II. The first important result is that the interference effect is not negligible even when w is very small, though not dramatic as in the $\gamma\gamma$ channel. For example, the case of $M_H = 300\,\mathrm{GeV}$, $c_{\beta-\alpha} = 0.1$, and $t_\beta = 10$ in Type

II, where $\Gamma_H/M_H = 0.2\%$, has $\Delta C \simeq -30\%$. The second result is that for the given t_β, $|\Delta C|$ decreases with M_H but increases again after the $t\bar{t}$ threshold. Before the $t\bar{t}$ threshold R increases much faster than w. After the $t\bar{t}$ threshold, w increases more sharply as the $t\bar{t}$ decay channel is opened.

The negative $c_{\beta-\alpha}$ case has very smooth and moderate variation of C. We have maximally 30% of ΔC for large t_β and light $M_H \simeq 200$ GeV or very heavy M_H. The positive $c_{\beta-\alpha}$ case allows the top-phobic lines and thus $C = 0$ line. Similar to $\gamma\gamma$ channel, the $c_{\beta-\alpha} = 0.4$ case in Type I has two $C = 0$ lines which are narrowly split near the top-phobic line. Near this top-phobic line $|\Delta C|$ is much enhanced since R is very suppressed. Note that large signal rate region, with small M_H and some deviation from the top-phobic line, has small ΔC. The $c_{\beta-\alpha} = 0.1$ case in Type II allows one $C = 0$ line, below which ΔC is negative. For $M_H = 200$ GeV and $t_\beta \simeq 5 \sim 10$, the reduction is about 50%.

We now investigate the interference effect on the future experimental sensitivity for the heavy Higgs boson via ZZ channel. We use the current experimental results on the heavy neutral Higgs search in the ZZ decay channel with $20.3\,\text{fb}^{-1}$ data at $8\,\text{TeV}$ from ATLAS collaboration [30]. The non-observation of any significant excess above the background is interpreted as an upper bound on $\sigma(gg \to H \to ZZ)$ as a function Higgs mass M_H. We project the results for 14 TeV LHC with $300\,\text{fb}^{-1}$ data by assuming that the statistical error is dominant [53, 54].

In Fig. 7, we show the 14 TeV LHC projections of the exclusion plots in (M_H, t_β) plane for $300\,\text{fb}^{-1}$ data. We set $c_{\beta-\alpha} = \pm 0.4$ in Type I and $c_{\beta-\alpha} = \pm 0.1$ in Type II. The hatched exclusion region is obtained by using naive NWA (without interference effect) while the green-colored exclusion region by mNWA (with interference effect). For Type I, we extend the exclusion region up to 1.5 TeV by applying a simple extrapolation. For $c_{\beta-\alpha} = -0.4$ the exclusion region covers the entire t_β region up to $M_H = 830$ GeV and the interference effect enlarges the exclusion region by $20 - 30$ GeV, $i.e.$, constructive interference. For $c_{\beta-\alpha} = 0.4$, there are two separate exclusion regions divided by top-phobic line. The upper (lower) region shows constructive (destructive) interference effect. Because of sizable top-quark Yukawa coupling above the top-phobic line, the large t_β region ($5 < t_\beta < 50$) up to $M_H = 800$ GeV also can be reached by LHC Run II data. As for type II, for $c_{\beta-\alpha} = 0.1$ ($c_{\beta-\alpha} = -0.1$) the interference effect is constructive (destructive).

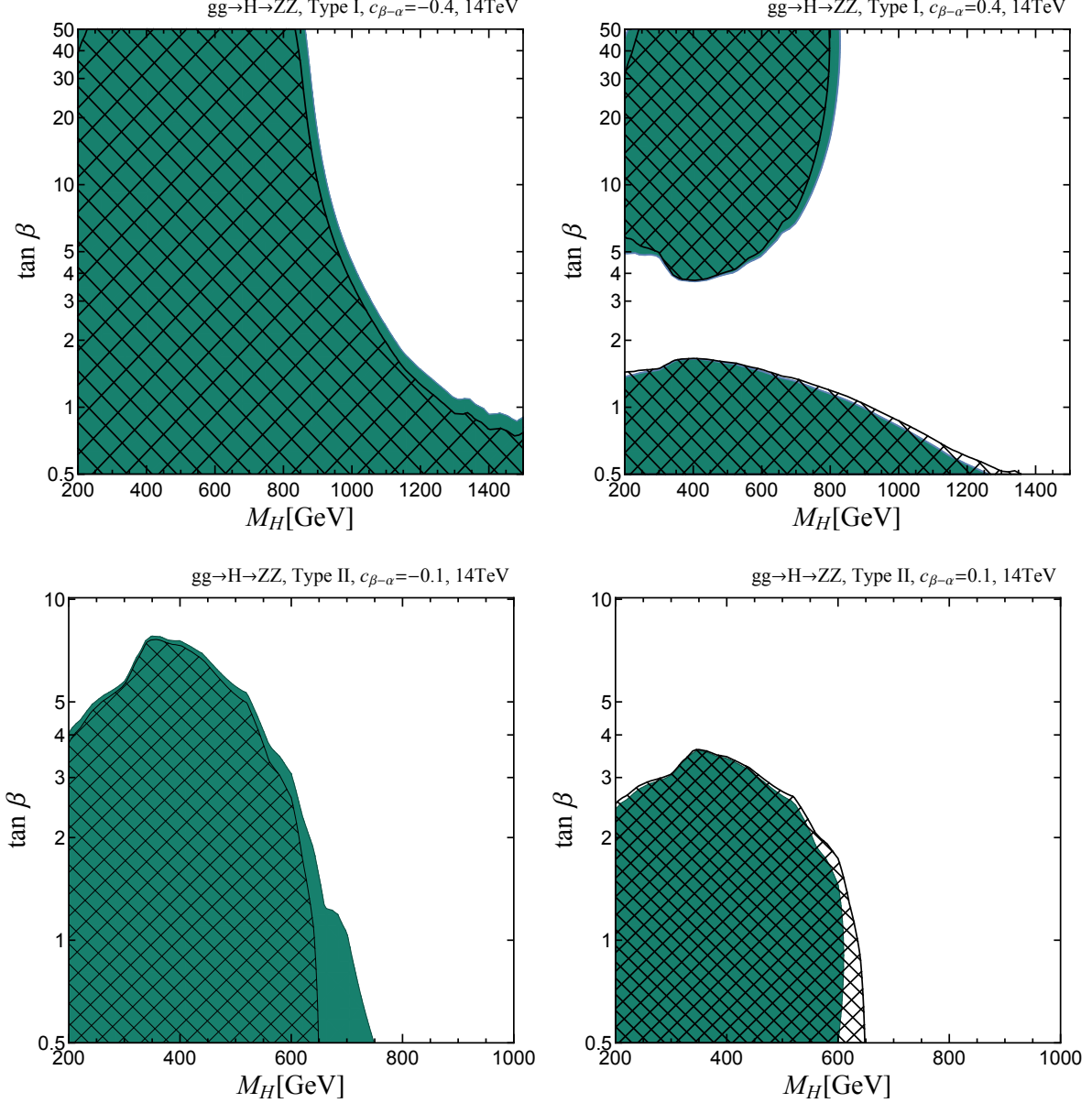Finally, we demonstrate the real-part interference effect by showing the contours of D^+

FIG. 7. Expected exclusion regions from ZZ resonance searches at the 14 TeV LHC with $300\,\mathrm{fb}^{-1}$, projected from the LHC 8 TeV results. The green regions include interference effects and the hatched regions are without interferences. We used the mNWA to obtain these results assuming that a resonance shape is approximately a BW peak.

and D^- in (M_H, t_β) plane: see Fig. 8. We take the case for $c_{\beta-\alpha} = 0.4$ in Type I at 14 TeV LHC, which brings about large real-part interference effects[5]. The behaviors of $D^\pm$ are quite similar to C: $D^\pm$ is large near top-phobic line where R is small. For D^-, the uncolored region indicates that the dip is shallower than the half-maximum of the BW peak. Even in this shallow dip region, D^+ can be up to 5, which is attributed to highly asymmetric m_{ZZ}

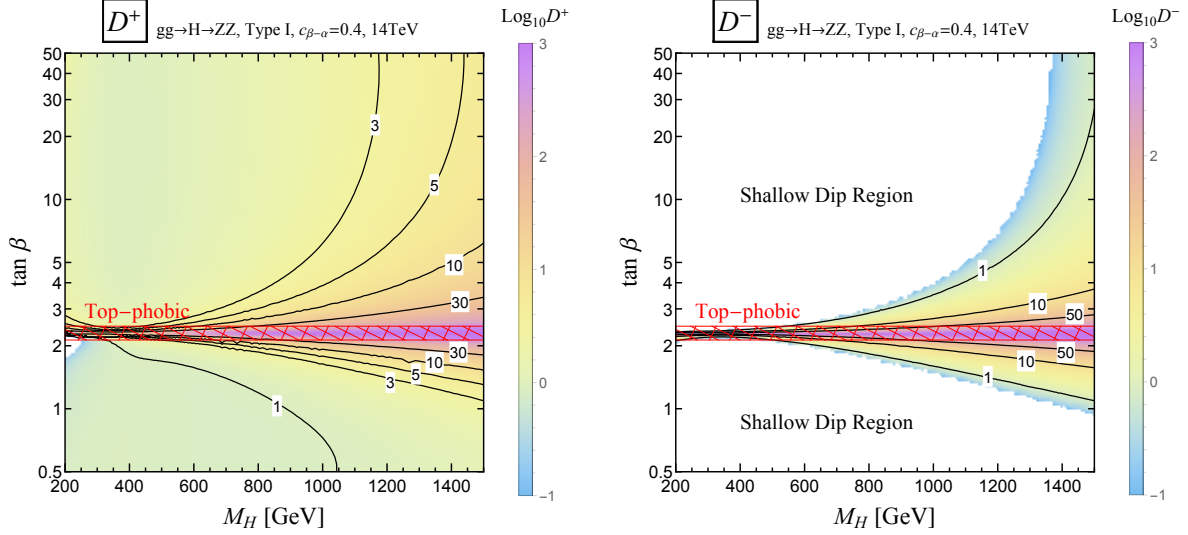[5] In other three cases, the real-part interference are mostly minor.

FIG. 8. Contours of D^+ (left) and D^- (right) in the $gg \to H \to ZZ$ process at the 14 TeV LHC for $c_{\beta-\alpha} = 0.4$ in Type I. $D^{\pm}$ are defined in Eq. (13). The red hatched region is around the top-phobic line such that $|\hat{y}_t^H| < 0.03$.
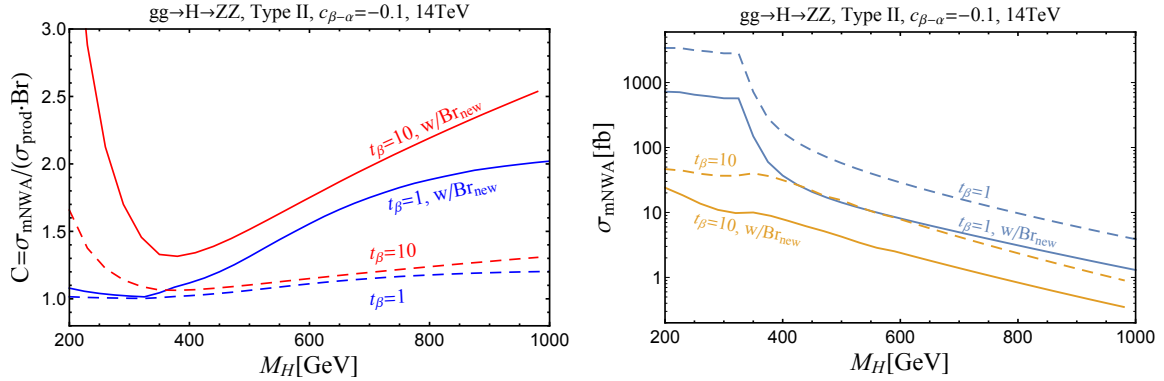

FIG. 9. Plots of C factor and σ_{mNWA} with respect to M_H for $gg \to H \to ZZ$ with some parameter choices. Solid lines include new decay channel with $\mathrm{Br_{new}} = 0.8$ while dashed lines do not.

distribution near $\hat{s} = M^2$. Note that the corresponding $|\Delta C|$ factor is less than $\sim 40\%$. The real-part interference can be more important, which is observable if the detector resolution is good enough to separate the peak from the dip. Once the dip is deep enough (colored region), both $D^{\pm}$ are larger than 1: a clear dip-peak ($c_\phi > 0$) or peak-dip ($c_\phi < 0$) shape is expected. The line-shape analysis can serve as another important probe for the heavy Higgs signal.
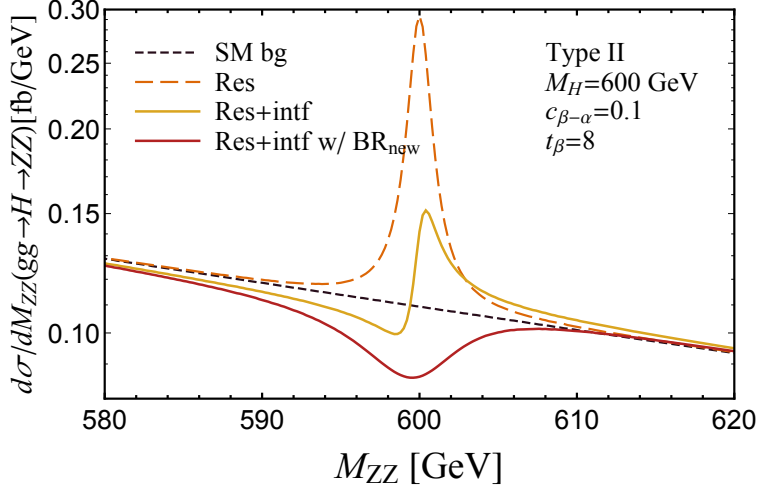
FIG. 10. Example ZZ invariant mass distribution of $gg \to H \to ZZ$ for given parameter choice. We show several results for comparison: the full result with interferences accounted for (yellow-solid), the pure BW result without interferences (orange-dashed), the full result with additional decay modes $\mathrm{Br_{new}} = 0.8$ (red-solid), and the continuum background $gg \to ZZ$ alone (black-dashed).

V.   ROLE OF TOTAL DECAY WIDTH

So far, we have assumed that the heavy H decays into the SM fermions or gauge bosons just as the SM Higgs boson. However, there exist additional decay channels like $H \to hh, ZA, W^{\pm}H^{\mp}$ in the 2HDM. As a benchmark scenario in Type II, we consider

$$c_{\beta-\alpha} = -0.1, \ t_\beta = 1.8, \ m_{12} = 240 \, \mathrm{GeV},$$
$$M_H = 550 \, \mathrm{GeV}, \ M_A = 350 \, \mathrm{GeV}, \ M_{H^+} = 350 \, \mathrm{GeV}, \tag{17}$$

which satisfies the constrains from $b \to s\gamma$ [55, 56], $\Delta\rho$ [57, 58] as well as the stability and perturbativity [37, 59]. Then additional decay channels have sizable branching ratio: $\mathrm{Br}(H \to hh) = 0.004$, $\mathrm{Br}(H \to ZA) = 0.25$, and $\mathrm{Br}(H \to W^{\pm}H^{\mp}) = 0.54$. Or 2HDM can be extended to include a dark matter candidate χ, allowing a new decay channel of $H \to \chi\chi$. The resulting increase in w shall affect the interference effect: ΔC is enhanced while $\mathrm{Br}(H \to ZZ)$ and thus σ_{mNWA} are reduced. Figure 9 shows the plots of C and σ_{mNWA} with $\mathrm{Br_{new}} = 0.8$ and some specific parameter choices in the ZZ channel. The magnitude of $|\Delta C|$ is significantly enhanced by a factor of about five. As discussed before, σ_{mNWA} is much reduced.

Finally, we illustrate how dramatically the resonance shape can be altered by changing the total width. Figure 10 shows the m_{ZZ} distribution for a benchmark point of $M_H = 600 \, \mathrm{GeV}$,

$c_{\beta-\alpha} = 0.1$ and $t_\beta = 8$ in Type II, which yields $R = 0.0063$, $\phi = -74°$, and $\sigma \cdot \mathrm{Br} \simeq 0.4\,\mathrm{fb}$. If H decays into the SM fermions and gauge bosons only, the total decay width is small ($w = 0.27\%$) and $\Delta C = -83\%$. The resonance shape is a suppressed dip-peak structure, as denoted by the yellow solid line. If we further allows a sizable branching ratio of a new decay channel like $\mathrm{Br_{new}} = 0.8$, the m_{ZZ} distribution shape changes into a new form, a pure dip (the red solid line). Three m_{ZZ} distribution lines clearly show that measuring the invariant mass distribution would serve as a multi-dimensional projection to extract the information of w, R and ϕ. This is to be compared with measuring the total signal rate only, just a single dimensional projection.

VI.   CONCLUSIONS

We have studied the resonance-continuum interference effects of the heavy neutral Higgs boson H of the nearly-aligned Type I and II 2HDM in the $\gamma\gamma$ and ZZ channels. Even for the H with a sub-percent width-to-mass ratio, the size and pattern of the interference effects can vary with underlying parameters and can be observably large.

For the parameter space where the ZZ resonance search at the LHC with $\sqrt{s} = 14\,\mathrm{TeV}$ is sensitive (particularly for small $t_\beta \lesssim 1$), the interference effects mildly modify the ZZ signal rate by $\mathcal{O}(10)\%$ and change the exclusion reach on the M_H by $\mathcal{O}(10)$ GeV. For example, the benchmark parameter $M_H = 300\,\mathrm{GeV}$, $c_{\beta-\alpha} = 0.1$, and $t_\beta = 10$ (yielding $\Gamma_H/M_H = 0.2\%$) modifies the ZZ signal rate by -30% from the interference. In this parameter space, we approximately treated the resonance shape as a BW peak and used the mNWA to estimate a new exclusion reach. In other words, we could use the C-factor to approximately quantify the interference effects (hence, on the signal rate).

In other parameter space where the ZZ signal rate is substantially smaller (such as near the top-phobic line), although it is unreachable for the LHC run at $14\,\mathrm{TeV}$, a resonance shape can be much more dramatically changed. Also for the $\gamma\gamma$ channel, signal rates are smaller and the LHC 14 TeV reach is absent in all parameter space, but the signal rates can be typically modified by $\mathcal{O}(100)\%$ due to interference effects. For the same parameter choice as in the previous paragraph, the $\gamma\gamma$ signal rate is modified by 400%. In these cases, one shall carry out a more careful collider study of resonance searches including the interference effects. Rather than doing this in this paper, we suggested a few variables that

can characterize a general resonance shape defined in Eqs. (10)-(13) and in Fig. 2. It will be worthwhile carrying out a dedicated future collider study.

The interference effects also grow with the resonance width. To illustrate this, we also considered a case with extra non-standard decay modes of the heavy Higgs boson. The increased width and correspondingly reduced signal could induce more significant interference effects in both channels. For example, with 80% new branching ratio, we find that the ZZ signal rate can be enhanced by a factor 2-3, but a more careful collider study including the modification of a resonance shape will be needed in this case.

From varying sizes of the interference with different signal rates, we verify a general result that we have discussed in Ref. [4]; the smaller the signal rate, the bigger the relative interference. The resonance-to-continuum ratio, approximately measured by R in Eq. (7), is another factor; the smaller the ratio, the bigger the relative interference. This is why the $\gamma\gamma$ channel experiences a bigger relative interference than the ZZ channel does. Looking forward, a 100 TeV pp collider and high-luminosity LHC data that can probe the parameter space with smaller signal rates will generically experience bigger interference effects.

[1] G. Aad *et al.* [ATLAS Collaboration], Phys. Lett. B **716**, 1 (2012); S. Chatrchyan *et al.* [CMS Collaboration], Phys. Lett. B **716**, 30 (2012).

[2] K. J. F. Gaemers and F. Hoogeveen, Phys. Lett. B **146**, 347 (1984).

[3] D. Dicus, A. Stange and S. Willenbrock, Phys. Lett. B **333**, 126 (1994) [hep-ph/9404359].

[4] S. Jung, J. Song and Y. W. Yoon, Phys. Rev. D **92**, no. 5, 055009 (2015) [arXiv:1505.00291].

[5] L. J. Dixon and M. S. Siu, Phys. Rev. Lett. **90**, 252001 (2003) [hep-ph/0302233].

[6] S. P. Martin, Phys. Rev. D **86**, 073016 (2012) [arXiv:1208.1533 [hep-ph]].

[7] L. J. Dixon and Y. Li, Phys. Rev. Lett. **111**, 111802 (2013) [arXiv:1305.3854 [hep-ph]].

[8] E. W. N. Glover and J. J. van der Bij, Nucl. Phys. B **321**, 561 (1989).

[9] D. A. Morris, T. N. Truong and D. Zappala, Phys. Lett. B **323**, 421 (1994) [hep-ph/9310244].

[10] P. Niezurawski, A. F. Zarnecki and M. Krawczyk, JHEP **0211**, 034 (2002) [hep-ph/0207294].

[11] J. M. Campbell, R. K. Ellis and C. Williams, JHEP **1110**, 005 (2011) [arXiv:1107.5569].

[12] N. Kauer and G. Passarino, JHEP **1208**, 116 (2012) [arXiv:1206.4803 [hep-ph]].

[13] N. Kauer, JHEP **1312**, 082 (2013) [arXiv:1310.7011 [hep-ph]].

[14] N. Kauer and C. O'Brien, arXiv:1502.04113 [hep-ph].

[15] C. Englert, I. Low and M. Spannowsky, Phys. Rev. D **91**, no. 7, 074029 (2015) [arXiv:1502.04678 [hep-ph]].

[16] N. Kauer, C. O'Brien and E. Vryonidou, arXiv:1506.01694 [hep-ph].

[17] M. Bonvini, F. Caola, S. Forte, K. Melnikov and G. Ridolfi, Phys. Rev. D **88**, no. 3, 034032 (2013) doi:10.1103/PhysRevD.88.034032 [arXiv:1304.3053 [hep-ph]].

[18] E. Asakawa, J. i. Kamoshita, A. Sugamoto and I. Watanabe, Eur. Phys. J. C **14**, 335 (2000) [hep-ph/9912373].

[19] L. J. Dixon and Y. Sofianatos, Phys. Rev. D **79**, 033002 (2009) [arXiv:0812.3712 [hep-ph]].

[20] J. L. Basdevant, E. L. Berger, D. Dicus, C. Kao and S. Willenbrock, Phys. Lett. B **313**, 402 (1993) [hep-ph/9211225].

[21] D. A. Dicus and S. S. D. Willenbrock, Phys. Rev. D **37**, 1801 (1988).

[22] W. Bernreuther, A. Brandenburg and M. Flesch, hep-ph/9812387.

[23] J. R. Ellis, J. S. Lee and A. Pilaftsis, Nucl. Phys. B **718**, 247 (2005) [hep-ph/0411379].

[24] M. Farina, Y. Grossman and D. J. Robinson, arXiv:1503.06470 [hep-ph].

[25] L. Bian, D. Liu, J. Shu and Y. Zhang, arXiv:1509.02787 [hep-ph].

[26] M. Beneke, A. P. Chapovsky, A. Signer and G. Zanderighi, Phys. Rev. Lett. **93**, 011602 (2004) [hep-ph/0312331].

[27] G. Aad *et al.* [ATLAS Collaboration], arXiv:1407.6583.

[28] CMS Collaboration [CMS Collaboration], CMS-PAS-HIG-14-006.

[29] S. Chatrchyan *et al.* [CMS Collaboration], Phys. Rev. D **89**, no. 9, 092007 (2014) [arXiv:1312.5353 [hep-ex]].

[30] G. Aad *et al.* [ATLAS Collaboration], arXiv:1507.05930 [hep-ex].

22

[31] N. Craig, F. D'Eramo, P. Draper, S. Thomas and H. Zhang, JHEP **1506**, 137 (2015) [arXiv:1504.04630 [hep-ph]].

[32] W. Bernreuther, M. Flesch and P. Haberl, Phys. Rev. D **58**, 114031 (1998) [hep-ph/9709284]. R. Frederix and F. Maltoni, JHEP **0901**, 047 (2009) [arXiv:0712.2355 [hep-ph]]. R. Barcelo and M. Masip, Phys. Rev. D **81**, 075019 (2010) [arXiv:1001.5456 [hep-ph]]. S. Moretti and D. A. Ross, Phys. Lett. B **712**, 245 (2012) [arXiv:1203.3746 [hep-ph]].

[33] The ATLAS collaboration [ATLAS Collaboration], ATLAS-CONF-2015-009.

[34] S. Chatrchyan *et al.* [CMS Collaboration], Phys. Rev. Lett. **111**, no. 21, 211804 (2013) [Phys. Rev. Lett. **112**, no. 11, 119903 (2014)] [arXiv:1309.2030 [hep-ex]].

[35] F. Caola and K. Melnikov, Phys. Rev. D **88**, 054024 (2013) [arXiv:1307.4935 [hep-ph]].

[36] V. Khachatryan *et al.* [CMS Collaboration], Phys. Lett. B **736** (2014) 64 [arXiv:1405.3455].

[37] G. C. Branco, P. M. Ferreira, L. Lavoura, M. N. Rebelo, M. Sher and J. P. Silva, Phys. Rept. **516**, 1 (2012).

[38] G. Belanger, B. Dumont, U. Ellwanger, J. F. Gunion and S. Kraml, Phys. Rev. D **88**, 075008 (2013); K. Cheung, J. S. Lee and P. Y. Tseng, JHEP **1305**, 134 (2013); C. W. Chiang and K. Yagyu, JHEP **1307**, 160 (2013); B. Grinstein and P. Uttayarat, JHEP **1306**, 094 (2013) [Erratum-ibid. **1309**, 110 (2013)]; O. Eberhardt, U. Nierste and M. Wiebusch, JHEP **1307**, 118 (2013); A. Celis, V. Ilisie and A. Pich, JHEP **1307**, 053 (2013). S. Chang, S. K. Kang, J. P. Lee, K. Y. Lee, S. C. Park and J. Song, JHEP **1305**, 075 (2013). S. Chang, S. K. Kang, J. P. Lee, K. Y. Lee, S. C. Park and J. Song, JHEP **1409**, 101 (2014) [arXiv:1310.3374 [hep-ph]].

[39] N. Craig, J. Galloway and S. Thomas, arXiv:1305.2424; A. Celis, V. Ilisie and A. Pich, JHEP **1312**, 095 (2013); JHEP **1404**, 128 (2014); P. S. B. Dev and A. Pilaftsis, JHEP **1412**, 024 (2014).

[40] L. Wang and X. F. Han, JHEP **1411**, 085 (2014) [arXiv:1404.7437 [hep-ph]].

[41] S. Kanemura, H. Yokoya and Y. J. Zheng, Nucl. Phys. B **886**, 524 (2014) [arXiv:1404.5835].

[42] J. Bernon, J. F. Gunion, Y. Jiang and S. Kraml, Phys. Rev. D **91**, 075019 (2015) [arXiv:1412.3385 [hep-ph]].

[43] B. Coleppa, F. Kling and S. Su, JHEP **1401**, 161 (2014) [arXiv:1305.0002 [hep-ph]].

[44] S. de Visscher, J. M. Gerard, M. Herquet, V. Lemaitre and F. Maltoni, JHEP **0908**, 042 (2009) [arXiv:0904.0705 [hep-ph]].

[45] S. Chang, S. K. Kang, J. P. Lee and J. Song, arXiv:1507.03618 [hep-ph].

[46] P. M. Ferreira, R. Guedes, M. O. P. Sampaio and R. Santos, JHEP **1412**, 067 (2014) [arXiv:1409.6723 [hep-ph]].

[47] V. Constantini, B. De Tollis and G. Pistoni, Nuovo Cimento 2A, 733 (1971).

[48] A. Djouadi, Phys. Rept. **459**, 1 (2008) [hep-ph/0503173].

[49] Z. Bern, A. De Freitas and L. J. Dixon, JHEP **0109**, 037 (2001) [hep-ph/0109078].

[50] H. L. Lai, M. Guzzi, J. Huston, Z. Li, P. M. Nadolsky, J. Pumplin and C.-P. Yuan, Phys. Rev. D **82**, 074024 (2010) [arXiv:1007.2241 [hep-ph]].

[51] M. Spira, hep-ph/9510347.

[52] J. Song and Y. W. Yoon, Phys. Rev. D **91**, no. 11, 113012 (2015) [arXiv:1412.5610 [hep-ph]].

[53] S. Jung and J. D. Wells, Phys. Rev. D **89**, no. 7, 075004 (2014) [arXiv:1312.1802 [hep-ph]].

[54] A. Djouadi, L. Maiani, A. Polosa, J. Quevillon and V. Riquer, JHEP **1506**, 168 (2015) [arXiv:1502.05653 [hep-ph]].

[55] F. Mahmoudi and O. Stal, Phys. Rev. D **81** (2010) 035016 [arXiv:0907.1791 [hep-ph]].

[56] T. Hermann, M. Misiak and M. Steinhauser, JHEP **1211**, 036 (2012).

[57] J. Gunion, et al., *The Higgs Hunter's Guide* (Addison-Wesley, New York, 1990).

[58] P. H. Chankowski, M. Krawczyk and J. Zochowski, Eur. Phys. J. C **11**, 661 (1999).

[59] S. Kanemura, Y. Okada, E. Senaha and C.-P. Yuan, Phys. Rev. D **70**, 115002 (2004) [hep-ph/0408364].